

Impact of ${}^7\text{Be}$ breakup on the ${}^7\text{Li}(p, n)$ neutron spectrum

C. V. Midhun,¹ M. M. Musthafa,^{1,*} S. V. Suryanarayana,² T. Santhosh,² A. Baishya,² P. N. Patil,³ A. Pal,² P. C. Rout,² S. Santra,² R. Kujur,² Antony Joseph,¹ Shaima A.,¹ Hajara. K.,¹ P. T. M. Shan,¹ Satheesh B.,⁴ Y. Sawant,² B. V. John,² E. T. Mirgule,² K. C. Jagadeesan,⁵ and S. Ganesan⁶

¹Department of Physics, University of Calicut, Calicut University, P.O Kerala 673635, India

²Nuclear Physics Division, Bhabha Atomic Research Centre, Mumbai 400085, India

³Department of Physics, Karnatak University, Dharwad, Karnataka 580003, India

⁴Department of Physics, Mahatma Gandhi Government Arts College, Mahe 673311, India

⁵Radiopharmaceuticals Division, Bhabha Atomic Research Centre, Mumbai 400085, India

⁶Formerly Raja Ramanna Fellow, Bhabha Atomic Research Centre, Mumbai 400085, India



(Received 19 July 2021; revised 27 September 2021; accepted 28 October 2021; published 16 November 2021)

The formation of continuum neutron distribution in ${}^7\text{Li}(p, n)$ has been identified as due to the coupling of the ${}^7\text{Be}$ breakup levels to the final state of the reaction. The continuum neutron spectra produced by the ${}^7\text{Li}(p, n)$ reaction has been estimated by measuring the double differential cross sections for continuum and resonant breakup of ${}^7\text{Be}$, through the ${}^7\text{Li}(p, n){}^7\text{Be}^*$ reaction at 21 MeV of proton energy. The breakup contributions from continuum and $5/2^-$, $7/2^-$ states of ${}^7\text{Be}$ have been identified. The measured double differential cross sections have been reproduced through continuum-discretized coupled channel-coupled reaction channel calculations. The cross sections were projected to neutron spectrum using the Monte Carlo approach and validated using experimentally measured ${}^3\text{He}$ gated neutron spectra. ${}^7\text{Li}(p, n)$ neutron spectrum at 20 MeV incident proton energy measured by McNaughton *et al.* [Nucl. Instrum. Methods **130**, 555 (1975)] has been reproduced by adapting estimated model parameters for the reaction.

DOI: [10.1103/PhysRevC.104.054606](https://doi.org/10.1103/PhysRevC.104.054606)

I. INTRODUCTION

Neutron induced reaction data, above 10 MeV, are having a renewed interest due to the nuclear data requirements for the design and safe operation of fusion reactors and accelerator driven systems (ADS) [1]. Activation analysis, using quasi-monoenergetic neutrons, is generally utilized for measuring cross sections for such studies. The ${}^7\text{Li}(p, n)$ channel is a promising source of such neutrons due to the quasi-monoenergetic behavior linearly up to 5 MeV. Further, the energy tunability and higher yield of this channel makes the ${}^7\text{Li}(p, n)$ the most used accelerator based neutron source for nuclear astrophysics and nuclear data measurements [2–4]. ${}^7\text{Li}(p, n)$ is also gaining attention as a compact accelerator neutron source (CANS) [3,5] in the fields of technology and medicine [6,7].

As the proton energy increases above 3.22 MeV, [1.64 MeV threshold for ${}^7\text{Li}(p, n)$ and 1.58 MeV breakup threshold for ${}^7\text{Be}$ to ${}^3\text{He}$ and α] the neutron distribution behaves as a continuum from 0 to $(E_p - 3.22 \text{ MeV})$, including the monoenergetic peaks corresponding to the population of ground and $1/2^-$ states. However, there are several measurements with ${}^7\text{Li}(p, n)$ neutrons, at proton energies above 15 MeV, for exploring the reactions having threshold greater than $(E_p - 5 \text{ MeV})$. This practice has been continued with the assumption that the neutrons contained in $(E_p - 5 \text{ MeV})$ to

$(E_p - 3.2 \text{ MeV})$ range is less than 1% of neutrons enclosed by n_0 and n_1 neutron colonies (corresponding to ground and $1/2^-$ states of ${}^7\text{Be}$, respectively). In some recent works, the extra contribution from the neutron continuum is being accounted for by the tailing correction methods [8,9].

So far there exist only a few measurements of the ${}^7\text{Li}(p, n)$ neutron spectrum above 5 MeV, the domain which the neutron continuum distribution is being prominently contributing to the neutron spectrum. These measurements were performed by McNaughton *et al.* [10] and Majerle *et al.* [11], with a thick ${}^{\text{nat}}\text{Li}$ target in the neutron time of flight mode, using the pulsed protons from cyclotron. There are some important works by Mashnik *et al.* [12], Meadows and Smith [13], and Drosig *et al.* [14], to theoretically model the neutron spectrum from the ${}^7\text{Li}(p, n)$ reaction, by taking neutron spectrum measured by McNaughton *et al.* as a reference. However, due to the lack of enough experimental data on ${}^7\text{Li}(p, n){}^7\text{Be}^* \rightarrow n + {}^3\text{He} + \alpha$, the neutron spectrum is not well reproduced by these attempts.

In the perspective of theoretical modeling, the neutron continuum distribution in the ${}^7\text{Li}(p, n)$ neutron spectrum, above the three-body breakup threshold, is considered to have emerged because of the coupling of continuum levels of ${}^7\text{Be}$ to the outgoing neutron wave function. These continuum levels are being considered as originated by the relative motion of α - ${}^3\text{He}$ internal structures of ${}^7\text{Be}$ above the breakup threshold of 1.58 MeV. Moreover, other than continuum states, the $5/2^-$, $7/2^-$ resonant states of ${}^7\text{Be}$ also contribute to the breakup. This makes the additional peak structures to the

*mmm@uoc.ac.in

end region of the continuum neutron spectrum. This implies that the shape of the continuum neutron spectrum has to be determined from the breakup cross section of ${}^7\text{Be}$ at the continuum energies above the breakup threshold. The continuum and resonant breakups of ${}^7\text{Be}$ have been measured by Chattopatyay *et al.* and theoretically reproduced through CDCC-CRC calculations [15]. A detailed theoretical exploration on the breakup of ${}^7\text{Be}$, based on CDCC calculations, is performed by Summers and Nunes [16] and Keeley *et al.* [17]. Mazzocco *et al.* experimentally studied the reaction dynamics of ${}^7\text{Be}$ in the field of ${}^{208}\text{Pb}$ and interpreted with FRESKO-CDCC calculations [18]. Kolata *et al.* have given a detailed review on the breakup of ${}^7\text{Be}$ based on recent measurements and theoretical studies [19]. Similarly, there are important measurements from the n_TOF collaboration on ${}^7\text{Be}(n, p)$ and ${}^7\text{Be}(n, \alpha)$ channels, which show a similar coupling of ${}^3\text{He}-\alpha$ breakup in the entrance channel [20,21]. A review on the breakup of ${}^7\text{Li}+p$ has been discussed by Pakou *et al.* [22]. However, in these works mentioned above, the entrance or exit conditions are different from the requirements of the present work and therefore, these measured cross sections cannot be directly adapted for explaining three-body continuum neutron spectrum from ${}^7\text{Li}(p, n)$.

The measurement of α - ${}^3\text{He}$ breakup cross sections from the continuum (resonant and nonresonant) states of ${}^7\text{Be}$ requires the coincidence detection of ${}^3\text{He}$ and α , where the sum of break-up threshold and relative energy between ${}^3\text{He}$ and α defines the excitation energy of ${}^7\text{Be}$. However due to the energy loss and energy and angular straggling of ${}^3\text{He}$ and α in the target, the reconstruction of excitation energies may sometimes become difficult. In a recent experiment using a 1.2 mg/cm^2 Li target the same problem was observed due to the issues of straggling and energy loss in the target as well as thicker ΔE detectors [23].

Based on the analysis of data from a previous attempt, the present experiment has been planned carefully and performed with a specially prepared thin ${}^{\text{nat}}\text{Li}$ target of $20\text{ }\mu\text{g/cm}^2$, sandwiched in between $5\text{ }\mu\text{g/cm}^2$ Al backing and $5\text{ }\mu\text{g/cm}^2$ carbon capping. It made the coincidence detection of ${}^3\text{He}$ and α and reconstruction of ${}^7\text{Be}$ excitation energy achievable due to a minimal energy and angular straggling. The double differential cross sections for ${}^7\text{Li}(p, n){}^7\text{Be}^* \rightarrow n + {}^3\text{He} + \alpha$ are measured and extended to the determination of the neutron spectrum. The determined cross section has been verified with the ${}^3\text{He}$ gated neutron spectrum measured through the time of flight technique. The details are presented in the following sections.

II. EXPERIMENTAL SETUP

The experiment was performed at BARC-TIFR Pelletron-Linac facility, Mumbai, India, using proton beam of 21 MeV. A specially fabricated $20\text{ }\mu\text{g/cm}^2$ ${}^{\text{nat}}\text{Li}$ target with $5\text{ }\mu\text{g/cm}^2$ Al backing and $5\text{ }\mu\text{g/cm}^2$ carbon capping has been used for the experiment. The schematic of the experiment is illustrated in Fig. 1. Two silicon detector telescopes, having $25\text{ }\mu\text{m}$ and $1500\text{ }\mu\text{m}$ ΔE - E pairs, were mounted at $+55^\circ$ and -55° with a distance of 7.5 cm from the target, to record the ejectile particles. Three EJ301 liquid organic scintillators

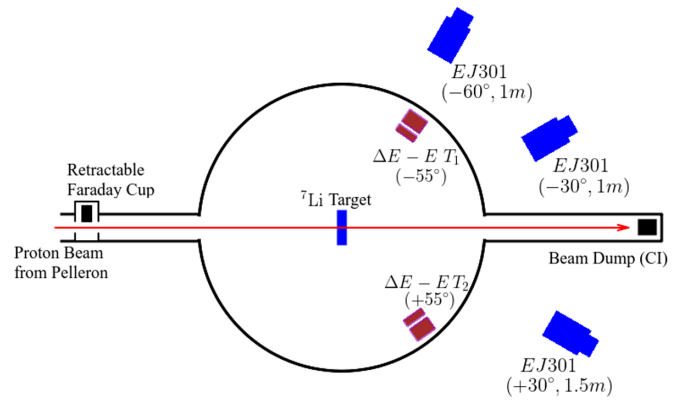


FIG. 1. Experimental setup.

having 12.7 cm diameter and 5 cm thick were configured for measuring neutrons. Two EJ301 detectors were positioned at -30° and -60° at a distance of 1 m from the target. The third detector was positioned at $+30^\circ$, 1.5 m from the target. The n - γ discrimination of the signal was performed using the Mesytec MPD-4 module. Further the neutron detectors were configured in time of flight (TOF) with start from ΔE detector signals. The telescopes were calibrated using ${}^{229}\text{Th}$ α sources. Neutron detector thresholds were set using ${}^{137}\text{Cs}$ sources and time to digital converters were calibrated using time calibrator module.

III. DATA ANALYSIS

A. Analysis of ${}^3\text{He}$ - α coincidences

The recorded events with $E - \Delta E$ correlation are illustrated in Fig. 2. A banana gate on the ${}^3\text{He}$ band resolves the α particle events coincident with ${}^3\text{He}$. Some of the α s are particles produced from the reaction ${}^6\text{Li}(p, \alpha){}^3\text{He}$. In addition many of the random events are also possible. Hence the events corresponding to the ${}^7\text{Li}(p, n){}^7\text{Be}^* \rightarrow n + {}^3\text{He} + \alpha$ reaction, which follow the three-body kinematics have been identified through a fixed radius nearest neighborhood approach [24,25].

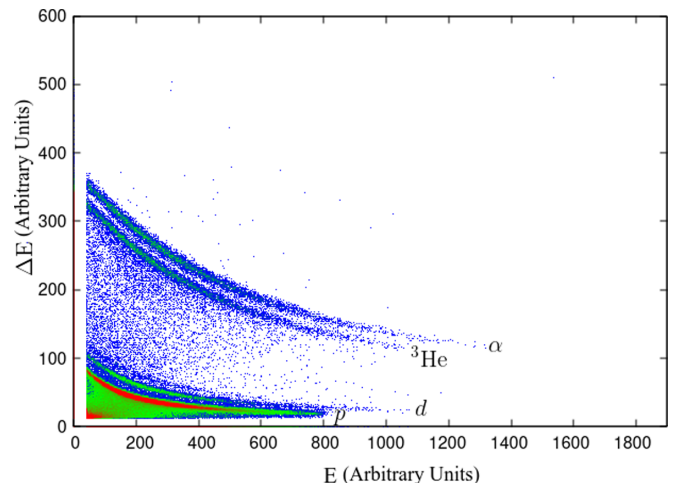


FIG. 2. ΔE - E correlation spectra measured by -55° telescope.

The kinematically allowed energies ($E_{3\text{He}}$ and E_α) corresponding to detector angles for the 21 MeV beam energy were taken as the quarry point. The constant radius is then considered as a window, and is taken as $\Delta = \sqrt{\sigma_{T1}^2 + \sigma_{T2}^2}$, where σ_{T1} and σ_{T2} are the respective energy resolution given by the two telescopes. This accepts ${}^3\text{He}$ - α coincidence events having both $E_{3\text{He}}$ and E_α that are inside the window. This makes the isolation of ${}^7\text{Li}(p, n){}^7\text{Be}^* \rightarrow n + {}^3\text{He} + \alpha$ events by removing ${}^6\text{Li}(p, \alpha){}^3\text{He}$ and other random coincidences. These types of events are addressed as ‘true events’. The other events, such as, $p + {}^{27}\text{Al} \rightarrow {}^3\text{He} + \alpha + {}^{21}\text{Ne}$ and $p + {}^{12}\text{C} \rightarrow {}^6\text{Li} + {}^3\text{He} + \alpha$ from aluminium and carbon present in the target, are not contributing to the present measurement as the thresholds for these channels are 22.6 MeV and 26 MeV, respectively. The ${}^6\text{Li}(p, \alpha){}^3\text{He}$ events are two orders lesser due to low cross section and lower percentage of ${}^6\text{Li}$ present in the target.

There are events, predicted by three-body kinematics, having E_α below the particle discrimination threshold with the coincident ${}^3\text{He}$ being above discrimination threshold, or vice versa. Such events were also reconstructed through the same nearest neighborhood approach, by considering the possible uncertainties in the measurement of energy. Thin gates were defined in the region of the ${}^3\text{He}/{}^4\text{He}$ band for which the kinematics predicts the possibility of counterparticle below discrimination threshold. A correlation plot between energies in telescope 1 vs telescope 2, under this gate, has been generated. The quarry point was defined in the same approach adapted for ‘true events’. The radius has been taken as $\Delta = \sqrt{\sigma_{\text{tel}}^2 + \Delta_{\text{gate}}^2 + \sigma_{\Delta E}^2 + E_{\text{strag}}}$, where σ_{tel} is the energy resolution of the telescope which identified the particle. Δ_{gate} is the energy width of the gate applied on the particle band and $\sigma_{\Delta E}$ is the energy resolution of the ΔE detector which detects the counterparticle. Further E_{strag} is the energy straggling of the low energy events inside the target. E_{strag} has been evaluated from the SRIM code, for the particular target geometry, however, found to be less compared to the ΔE resolution. The circle defined by the center as a query point and radius Δ together forms a gate for counterparticle events and these events have been projected towards the ΔE energy. The centroid of the projected distribution is taken as the average energy of the counterparticle. Such events will be addressed as reconstructed events. A typical $E_{3\text{He}}-\Delta E$ correlation with defined circle for event selection is presented in Fig. 3.

The energy state of ${}^7\text{Be}$ was reconstructed by adding $E_{3\text{He}}$ and E_α . The doubly differentiated cross sections for the laboratory folding angle between ${}^3\text{He}$ $-\alpha = 110^\circ$ and the neutron energy spectrum have been constructed through the energetics as

$$E_n = E_{\text{beam}} - E_\alpha - E_{3\text{He}} + E_{\text{loss}} + Q, \quad (1)$$

where E_n is the neutron energy, E_{loss} is the energy loss of the particle inside the target, and Q is the Q value for three-body breakup (-3.23 MeV).

B. FRESKO calculations

Continuum discretized coupled channels (CDCC) calculations using FRESKO [26] are performed for reproducing

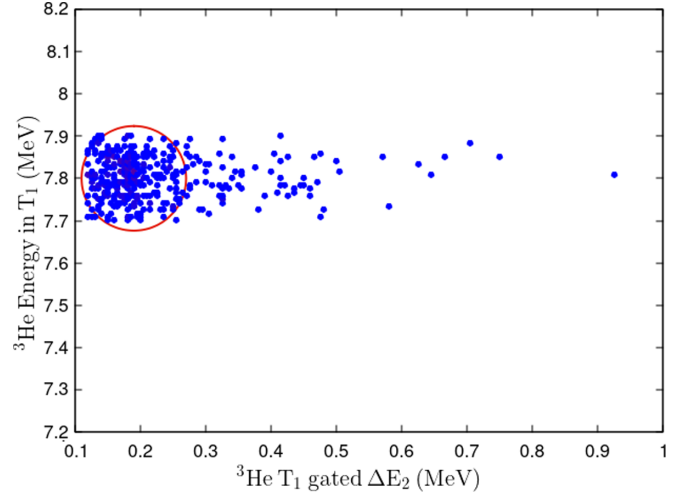


FIG. 3. An example energy correlation plot of the energy measured in -55° versus energy of resolved ${}^3\text{He}$ in $+55^\circ$, for the coincidence events, used for reconstruction of α s below the discrimination threshold. Red circle indicates the constant radius (Δ) window about kinematically defined query point

the measured double differential cross sections for ${}^7\text{Li}(p, n){}^7\text{Be}^* \rightarrow n + {}^3\text{He} + \alpha$. The energy distribution of the emitted neutron is considered as arising due to the coupling of continuum states of ${}^7\text{Be}$ to the outgoing neutron levels. The problem has been defined as $p + {}^7\text{Li}$ (where ${}^7\text{Li}$ as $\alpha + t$ cluster) for the entrance channel and ${}^7\text{Be} + n$ (where ${}^7\text{Be}$ as $\alpha + {}^3\text{He}$ cluster) as exit channel mass partitions. The continuum states corresponding to the ${}^7\text{Be}$, above the α - ${}^3\text{He}$ breakup threshold (1.59 MeV) have been generated and discretized with respect to the α - ${}^3\text{He}$ relative momentum. The relative momentum ($\hbar k$) up to 5 fm^{-1} was considered for the analysis. This range was discretized into a number of bins in the interval of $\Delta k = 0.125 \text{ fm}^{-1}$. The spin corresponding to each bin has been obtained as the vector sum of α - ${}^3\text{He}$ relative angular momentum and spin of ${}^3\text{He}$. The optical potentials corresponding to $p + {}^7\text{Li}$ have been taken from [27–31] and the $\alpha + n$ optical potentials have been obtained from [32]. The potentials corresponding to ${}^3\text{He} + n$ have been obtained by fitting the angular distribution data reported by Drog [33]. A differential cross section corresponding to each continuum bin has been generated through CDCC calculations. An alternative CDCC + CRC calculation was performed to account for the ${}^7\text{Be}^* \rightarrow {}^3\text{He} + \alpha$ angular distribution, including resonant breakup contribution from $7/2^-$ and $5/2^-$ levels. The overlaps from continuum states produced by $\alpha + {}^3\text{He}$ and ${}^6\text{Li} + p$, above the breakup thresholds of 1.59 and 5.6 MeV are considered for the estimation of breakup from the resonant levels. The spectroscopic amplitudes corresponding to continuum and resonant breakups have been adapted from the references, however the overlaps are different in those cases and in the above, a fine optimization has been performed [15]. The calculated cross sections were cascaded to obtain the double differentiated cross sections corresponding to the ${}^7\text{Li}(p, n){}^7\text{Be}^* \rightarrow {}^3\text{He} + \alpha$ reaction channel. The cascaded cross sections were

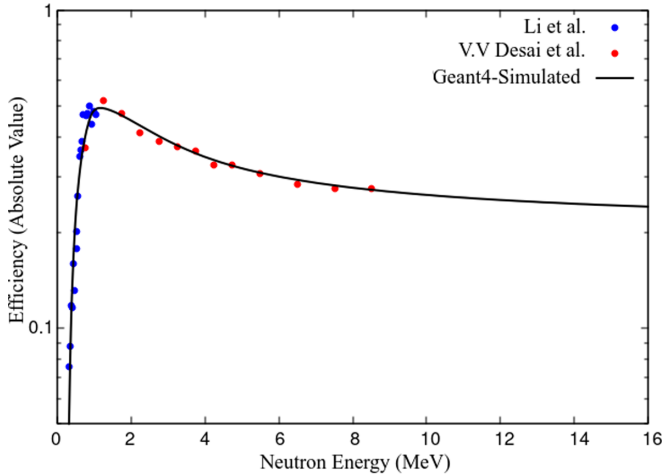


FIG. 4. Neutron energy-efficiency plot for EJ301 liquid scintillator.

projected for the laboratory, corresponding to 110° , via three-body kinematics, to meet the experimental conditions. This conversion has been performed with the three-body kinematics calculator available in the nuclear reaction video project with utilizing the relative energy filter option [34].

C. Evaluation and validation of neutron spectrum

The full neutron spectrum has been generated through the Monte Carlo approach using the FRESKO calculated cross sections, in which the double differential part was matched with the experimental cross sections. This neutron spectrum has been validated through a ^3He gated neutron spectrum measured in the experiment. The ^3He event gated neutron bands, identified from the TOF-PSD correlation plots corresponding to each neutron detectors, were projected onto the TOF axis. The projected histogram has been converted to the energy spectrum by time calibration. Since the neutron spectrum is extending up to 16 MeV, the energy efficiencies for neutron detectors were simulated using GEANT4, up to 16 MeV, and compared with previously measured efficiencies [35]. The energy-efficiency plot generated for EJ-301 neutron scintillators is presented in Fig. 4.

In order to validate the theoretical estimates of neutron spectra based on the measured breakup cross sections, for the 21 MeV proton energy case, we proceeded as follows. The full neutron spectrum has been generated through the Monte Carlo approach using a three-step procedure. (a) As described in Sec. III B, the CDCC+CRC calculations using FRESKO were carried out to obtain theoretical estimates of breakup cross sections and the double differential cross sections which are matched with the experimentally measured cross sections by the events in telescopes. (b) Using the FRESKO results of cross sections, the neutron spectra corresponding to 30° and 60° neutron events which are in coincidence with ^3He at 55° , have been generated through the Monte Carlo approach. (c) From experimentally recorded events in the EJ301 detectors, we obtained ^3He events at 55° gated neutron spectra. The vali-

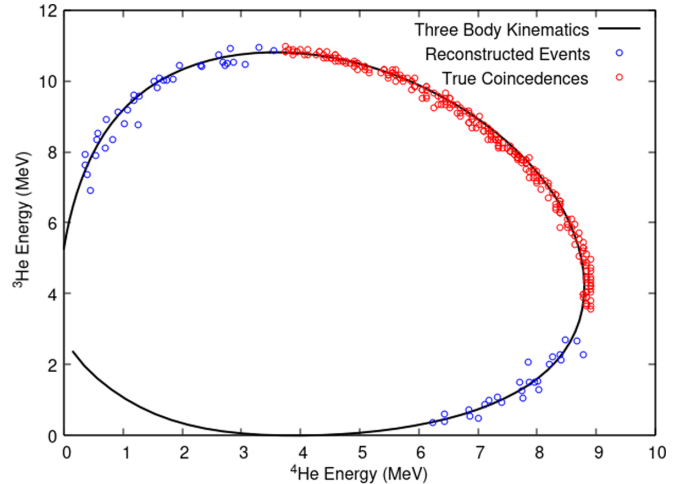


FIG. 5. The true coincidence and reconstructed events comparison with three-body kinematics, projected to the fragments at $+55^\circ$ and -55°

dation of theoretical estimates by comparing (b) and (c), i.e., the Monte Carlo generated with the experimentally measured neutron spectra. This procedure of validation has been carried out also for 20 MeV proton energy. Since we did not measure for 20 MeV proton energy, we proceed to use the experimental data reported by McNaughton *et al.* using a thicker Li target. We performed a set of FRESKO followed by Monte Carlo calculations for 20 MeV along with SRIM calculations to account for the thick target effect and these calculations reproduced the spectrum reported by McNaughton *et al.*

Neutron spectra corresponding to 30° and 60° neutron events, in coincidence with 55° ^3He , have been generated through the Monte Carlo approach based on FRESKO calculated cross sections. This spectra have been compared with the experimentally measured neutron spectra, for the validation of the theoretical estimates based on the measured breakup cross sections. Similarly, another set of FRESKO and Monte Carlo calculations has been performed for 20 MeV proton energy to reproduce the spectrum reported by McNaughton *et al.*, along with SRIM [36] calculations to account for the thick target effect. The n_0 and n_1 component to the neutron spectra have been calculated using FRESKO including the ground ($3/2^-$) and 429 keV ($1/2^-$) states. FRESKO calculated cross sections for ground ($3/2^-$) and 429 keV ($1/2^-$) states were validated with TENDL-2019 evaluated cross sections for $^7\text{Li}(p, n)^7\text{Be}$ [37].

IV. RESULTS AND DISCUSSION

Measured energy correlation for $^3\text{He}-\alpha$ agrees well with the three-body kinematics predicted for the $^7\text{Li}(p, n)^7\text{Be}^* \rightarrow n + ^3\text{He} + \alpha$ reaction. Measurements are limited to a $^3\text{He}-\alpha$ folding angle of 110° in the laboratory frame, however, events got registered to a reasonable statistics. The $^3\text{He}-\alpha$ energy correlation, along with three-body kinematics, is presented in Fig. 5. Measured double differential cross sections for the breakup corresponding to continuum states of ^7Be are illustrated as locally averaged effective histogram

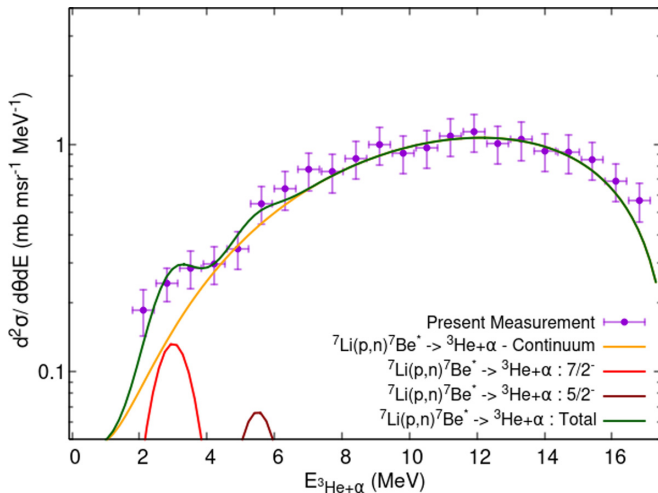


FIG. 6. The measured double differential cross sections for ${}^7\text{Li}(p, n){}^7\text{Be}^* \rightarrow n + {}^3\text{He} + \alpha$, and CDCC-CRC calculated continuum and resonant state cross sections (for the laboratory folding angle of 110°).

values in Fig. 6, along with FRESKO-CDCC calculations for ${}^7\text{Li}(p, n){}^7\text{Be}^* \rightarrow n + {}^3\text{He} + \alpha$. The comparison of measured double differential cross section with CDCC-CRC results shows a good agreement and illustrates the physics of neutron continuum formation in this typical reaction channel. Based on CDCC-CRC analysis, it is well understood that the continuum neutron distribution is formed due to the coupling of breakup levels to the ${}^7\text{Be} + n$ state. Other than the continuum, there exist $7/2^-$ and $5/2^-$ levels above breakup threshold, which contribute as the resonant breakups. In the present study, breakup contributions from these resonant levels are observed with a lesser statistics. However, these peaks are being reproduced with CDCC-CRC calculations. The spectroscopic amplitudes (SA) of 0.26, 1, and 0.57 have been used in reproducing continuum, $7/2^-$, and $5/2^-$ contributions, respectively.

The Monte Carlo based calculation for 0° neutrons has been performed using the CDCC-CRC calculated cross section with parameters obtained through matching the experimentally measured double differential cross sections. The CRC were considered for accounting the resonant breakup contribution. The estimated 0° neutron spectrum, corresponding to the breakup is presented in Fig. 7. This shows the contribution from $7/2^-$ (4.57 MeV) and $5/2^-$ (6.73 and 7.21 MeV) levels as Gaussian peaks. Due to the overlaps of the continuum levels to the resonant states, the width of the resonant breakup neutron colonies is large.

The validation of theoretically calculated neutron spectra has been performed with experimentally measured 55° - ${}^3\text{He}$ gated neutron spectrum at 30° and 60° . The theoretical spectra for these angles are generated through the Monte Carlo approach over the theoretical cross sections, as described above. The comparison of the theoretically evaluated neutron spectrum with 55° - ${}^3\text{He}$ gated neutron spectrum at 30° and 60° is presented in Fig. 8. The comparison shows that the theoretically generated neutron spectra well reproduce the

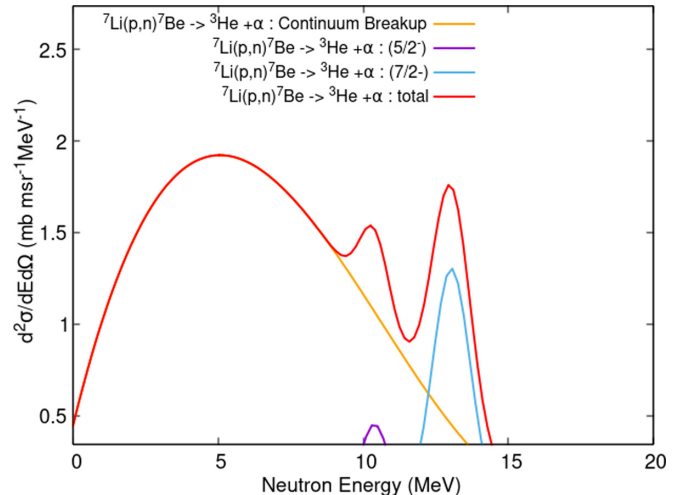


FIG. 7. The simulated 0° breakup neutron spectrum at 21 MeV, having continuum and resonance contributions.

experimental neutron spectrum within the counting statistics of the neutrons per energy bin.

The comparison of theoretical neutron spectra for 20 MeV of proton energy and the neutron spectra reported by McNaughton *et al.* is illustrated in Fig. 9. This shows the theoretical calculations, with parameters used for reproducing the double differential cross section of ${}^7\text{Li}(p, n){}^7\text{Be}^* \rightarrow n + {}^3\text{He} + \alpha$ are quite apt for generating the breakup neutron spectrum from the $p + {}^7\text{Li}$ system. The n_0 and n_1 neutron colonies are well reproduced by the FRESKO calculations, optimized and validated with respect to TENDL-2019 evaluations.

The continuum neutron colony, emerging due to the coupling of continuum levels generated by the $\alpha + {}^3\text{He}$ cluster structure to the ${}^7\text{Be} + n$ final state, has been qualitatively measured by the present study. Effect of coupling of $\alpha + {}^3\text{He}$ continuum levels makes a neutron distribution from 0 MeV to

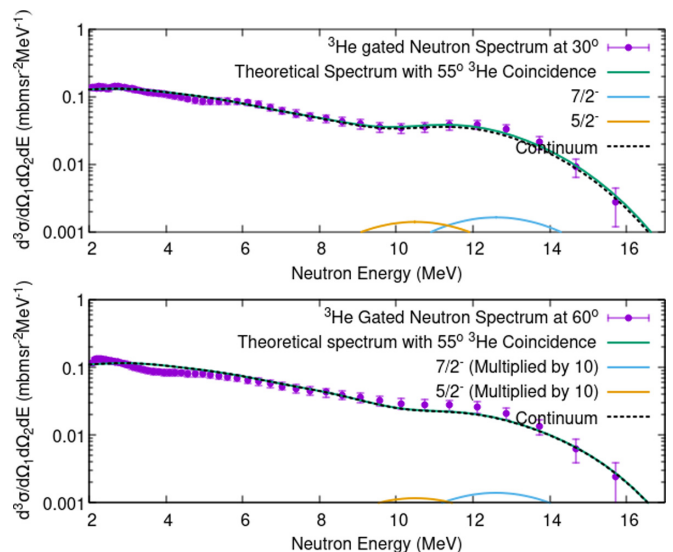


FIG. 8. The comparison of ${}^3\text{He}$ gated neutron spectra with theoretical spectra.

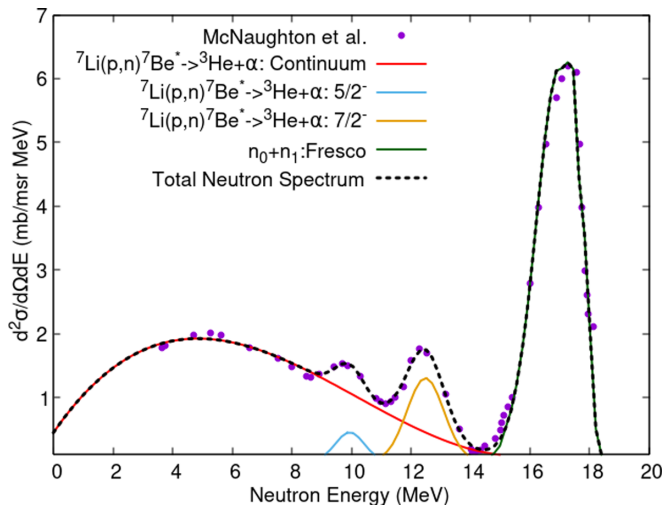


FIG. 9. Comparison of evaluated neutron spectrum with the spectrum reported by McNaughton *et al.* for 20 MeV.

$E_{\text{beam}} - Q$, where Q is the sum of the Q value for ${}^7\text{Li}(p, n)$ and the breakup threshold of ${}^7\text{Be}$ to α and ${}^3\text{He}$. Further, at the high energy tail of the breakup continuum, two additional peaks are formed, corresponding to the $7/2^-$ and $5/2^-$ resonance levels of ${}^7\text{Be}$, above the breakup threshold. The overlaps of breakup levels of ${}^7\text{Be}$ produced by ${}^3\text{He} + \alpha$ and ${}^6\text{Li} + p$ structures, above 1.59 and 5.60 MeV, produce a broadening of the resonance neutron colonies. However, for the practical use, the neutron distribution at the lower energy will be different, due to the presence of satellite neutrons as recommended by Drosg evaluations [14]. The satellite neutron distributions are

formed through multiple scattering of neutrons, which are highly dependent on the experimental setup. However, the present study is concluded without accounting the satellite neutrons, formed at lower energies.

V. SUMMARY

The formation of the continuous neutron distribution for the ${}^7\text{Li}(p, n)$ reaction at 21 MeV proton energy has been identified as the overlap of continuum levels generated by $\alpha + {}^3\text{He}$ clusters of ${}^7\text{Be}$ above the breakup threshold. This has been verified by measuring the double differential cross sections for three-body breakup at 21 MeV of proton energy. The measured double differential cross sections have been reproduced through FRESKO calculations by adding the coupling of continuum generated by $\alpha + {}^3\text{He}$ to the ${}^7\text{Be} + n$ final state. The neutron spectrum has been simulated through the Monte Carlo approach using FRESKO calculated cross sections. These neutron spectra have been validated using the experimentally measured ${}^3\text{He}$ gated spectrum and McNaughton's spectrum reported for 20 MeV.

ACKNOWLEDGMENTS

The support of BARC-TIFR Pelletron-LINAC group during the experiment is acknowledged. The authors acknowledge the staff in TIFR Target Laboratory in the development of the sandwiched Li target for the experiment. The authors acknowledge, A. K. Bhakshi and Rupali Pal, RP&AD BARC, Mumbai and A. Shanbhag, Health Physics Division, BARC for their kind support during the experiment. This study is part of the project supported by DAE-BRNS, Sanction Order No. 36(6)/14/30/2017-BRNS/36204.

- [1] S. Ganesan, Nuclear data requirements for accelerator driven sub-critical systems—a roadmap in the indian context, *Pramana - J. Phys.* **68**, 257 (2007).
- [2] R. Pachua, B. Lalremruata, N. Otuka, L. R. Hlondo, L. R. M. Punte, and H. H. Thanga, Thick and thin target ${}^7\text{Li}(p, n){}^7\text{Be}$ neutron spectra below the three-body breakup reaction threshold, *Nucl. Sci. Eng.* **187**, 70 (2017).
- [3] O. Sgouros, V. Soukeras, and Pakou, Low energy proton induced reactions with weakly bound nuclei for application purposes, *Eur. Phys. J. A* **57**, 125 (2021).
- [4] M. Tessler, M. Friedman, S. Schmidt, A. Shor, D. Berkovits, D. Cohen, G. Feinberg, S. Fiebiger, A. Krása, M. Paul, R. Plag, A. Plompen, and R. R., Neutron energy spectra and yields from the ${}^7\text{Li}(p, n)$ reaction for nuclear astrophysics, *J. Phys.: Conf. Ser.* **665**, 012027 (2016).
- [5] M. Tessler *et al.*, Stellar 30 keV neutron capture in ${}^{94,96}\text{Zr}$ and the ${}^{90}\text{Zr}(\gamma, n){}^{89}\text{Zr}$ photonuclear reaction with a high power liquid lithium target, *Phys. Lett. B* **751**, 418 (2015).
- [6] M. S. Herrera, G. A. Moreno, and A. J. Kreiner, Revisiting the ${}^7\text{Li}(p, n){}^7\text{Be}$ reaction near threshold, *Appl. Radiat. Isot.* **88**, 243 (2014).
- [7] I. Mardor *et al.*, The Soreq applied research accelerator facility (SARAF): Overview, research programs and future plans, *Eur. Phys. J. A* **54**, 91 (2018).
- [8] S. Parashari, S. Mukherjee, H. Naik, S. V. Suryanarayana, R. Makwana, B. K. Nayak, and N. L. Singh, Measurement of the ${}^{58}\text{Ni}(n, p){}^{58}\text{Co}$ and ${}^{58}\text{Ni}(n, 2n){}^{57}\text{Ni}$ reaction cross-sections for fast neutron energies up to 18 MeV, *Eur. Phys. J. A* **55**, 51 (2019).
- [9] D. L. Smith, A. J. M. Plompen, and V. Semkova, Correction for low energy neutrons by spectral indexing, *OECD NEA/WPEC-19* **19**, 155 (2005), <https://www.oecd-nea.org/upload/docs/application/pdf/2019-12/volume19.pdf>.
- [10] M. McNaughton, N. King, F. Brady, J. Romero, and T. Subramanian, Measurements of ${}^7\text{Li}(p, n)$ and ${}^9\text{Be}(p, n)$ cross sections at 15, 20 and 30 MeV, *Nucl. Instrum. Methods* **130**, 555 (1975).
- [11] M. Majerle, P. Bém, J. Novák, E. Šimečková, and M. Štefánik, Au, Bi, Co and Nb cross-section measured by quasimonoeenergetic neutrons from $p + {}^7\text{Li}$ reaction in the energy range of 18–36 MeV, *Nucl. Phys. A* **953**, 139 (2016).
- [12] S. G. Mashnik, M. B. Chadwick, P. G. Young, R. E. MacFarlane, and L. S. Waters, ${}^7\text{Li}(p, n)$ Nuclear Data Library for Incident Proton Energies to 150 MeV, Tech. Report No. LA-UR-00-1067 (Los Alamos National Laboratory, Los Alamos, NM, 2000).
- [13] J. Meadows and D. Smith, *Protons from Neutron Bombardment of Natural Lithium*, Tech. Report No. ANL-7938 (Argonne National Laboratory, Argonne, Illinois, 1972).

- [14] M. Drosig, Sources of variable energy monoenergetic neutrons for fusion-related applications, *Nucl. Sci. Eng.* **106**, 279 (1990).
- [15] D. Chattopadhyay, S. Santra, A. Pal, A. Kundu, K. Ramachandran, R. Tripathi, T. N. Nag, and S. Kailas, Direct and resonant breakup of radioactive ${}^7\text{Be}$ nuclei produced in the ${}^{112}\text{Sn}({}^6\text{Li}, {}^7\text{Be})$ reaction, *Phys. Rev. C* **102**, 021601(R) (2020).
- [16] N. C. Summers and F. M. Nunes, ${}^7\text{Be}$ breakup on heavy and light targets, *Phys. Rev. C* **70**, 011602(R) (2004).
- [17] N. Keeley, K. W. Kemper, and K. Rusek, ${}^7\text{Be}$ versus ${}^7\text{Li}$: the influence of breakup threshold on the dynamic polarization potential, *Phys. Rev. C* **66**, 044605 (2002).
- [18] M. Mazzocco *et al.*, Elastic scattering for the ${}^8\text{B}$ and ${}^7\text{Be} + {}^{208}\text{Pb}$ systems at near-Coulomb barrier energies, *Phys. Rev. C* **100**, 024602 (2019).
- [19] J. J. Kolata, V. Guimarães, and E. F. Aguilera, Elastic scattering, fusion, and breakup of light exotic nuclei, *Eur. Phys. J. A* **52**, 123 (2016).
- [20] L. M. Damone *et al.*, ${}^7\text{Be}(n, p){}^7\text{Li}$ Reaction and the Cosmological Lithium Problem: Measurement of the Cross Section in a Wide Energy Range at n_tof at CERN, *Phys. Rev. Lett.* **121**, 042701 (2018).
- [21] M. Barbagallo *et al.*, ${}^7\text{Be}(n, \alpha){}^4\text{He}$ Reaction and the Cosmological Lithium Problem: Measurement of the Cross Section in a Wide Energy Range at n_tof at CERN, *Phys. Rev. Lett.* **117**, 152701 (2016).
- [22] A. Pakou, O. Sgouros, V. Soukeras, and F. Cappuzzello, Global descriptions and decay rates for continuum excitation of weakly bound nuclei, *Eur. Phys. J. A* **57**, 25 (2021).
- [23] S. V. Suryanarayana, E. T. Mirgule *et al.*, Continuum neutrons in ${}^7\text{Li}(p, n)$ reaction (private communication).
- [24] A. De Simone and T. Jacques, Guiding new physics searches with unsupervised learning, *Eur. Phys. J. C* **79**, 289 (2019).
- [25] A. Collaboration, Observation of a new particle in the search for the standard model Higgs boson with the atlas detector at the LHC, *Phys. Lett. B* **716**, 1 (2012).
- [26] I. J. Thompson, Coupled reaction channels calculations in nuclear physics, *Comput. Phys. Rep.* **7**, 167 (1988).
- [27] A. Pakou, V. Soukeras, F. Cappuzzello, L. Acosta, C. Agodi, X. Aslanoglou, S. Calabrese, D. Carbone, M. Cavallaro, A. Foti, N. Keeley, G. Marquinez-Duran, I. Martel, M. Mazzocco, C. Parascandolo, D. Pierroutsakou, K. Rusek, O. Sgouros, E. Strano, and V. A. B. Zagatto, Probing the cluster structure of ${}^7\text{Li}$ via elastic scattering on protons and deuterons in inverse kinematics, *Phys. Rev. C* **94**, 014604 (2016).
- [28] G. Freier, E. Lampi, W. Sleator, and J. H. Williams, Angular distribution of 1- to 3.5-MeV protons scattered by He^4 , *Phys. Rev.* **75**, 1345 (1949).
- [29] P. D. Miller and G. C. Phillips, Scattering of protons from helium and level parameters in Li^5 , *Phys. Rev.* **112**, 2043 (1958).
- [30] J. E. Brolley, T. M. Putnam, L. Rosen, and L. Stewart, Hydrogen-helium isotope elastic scattering processes at intermediate energies, *Phys. Rev.* **117**, 1307 (1960).
- [31] R. Kankowsky, J. Fritz, K. Kilian, A. Neufert, and D. Fick, Elastic scattering of polarized protons on tritons between 4 and 12 MeV, *Nucl. Phys. A* **263**, 29 (1976).
- [32] G. Satchler, L. Owen, A. Elwyn, G. Morgan, and R. Walter, An optical model for the scattering of nucleons from 4He at energies below 20 MeV, *Nucl. Phys. A* **112**, 1 (1968).
- [33] M. Drosig, R. A. Ortiz, and P. W. Lisowski, Neutron interactions with 3He revisited-i: Elastic scattering around and beyond 10 MeV, *Nucl. Sci. Eng.* **172**, 87 (2012).
- [34] V. Zagrebaev *et al.*, Nuclear reaction video project, 3-body kinematics of nuclear reactions, http://nrv.jinr.ru/nrv/webnrv/kinematics/three_body.php.
- [35] V. V. Desai, B. K. Nayak, A. Saxena, S. V. Suryanarayana, and R. Capote, Prompt fission neutron spectra in fast-neutron-induced fission of ${}^{238}\text{U}$, *Phys. Rev. C* **92**, 014609 (2015).
- [36] J. F. Ziegler, Srim-2003, *Nucl. Instrum. Methods Phys. Res. B* **219–220**, 1027 (2004), proceedings of the 16th International Conference on Ion Beam Analysis.
- [37] A. Koning, D. Rochman, J.-C. Sublet, N. Dzysiuk, M. Fleming, and S. van der Marck, TENDL: Complete nuclear data library for innovative nuclear science and technology, *Nucl. Data Sheets* **155**, 1 (2019), special issue on nuclear reaction data.